A

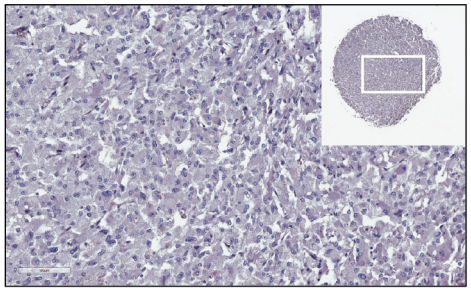

Anti Rabbit Isotype control

B

Sex	Age	Organ	Pathology diagnosis	Grade	Stage	TNM	Type
F	55	Colon	Adenocarcinoma	1	IIIB	T3N1M0	Malignant
F	62	Colon	Adenocarcinoma	1	IIB	T3N0M0	Malignant
M	48	Colon	Adenocarcinoma	1	I	T2N0M0	Malignant
M	56	Colon	Adenocarcinoma	–	IIA	T3N0M0	Malignant
M	27	Colon	Adenocarcinoma	1	I	T2N0M0	Malignant
F	68	Colon	Adenocarcinoma	1	IIIB	T4N2M0	Malignant
M	61	Colon	Adenocarcinoma	1	IIB	T4N0M0	Malignant
M	50	Colon	Adenocarcinoma	2	IIA	T3N0M0	Malignant
F	62	Colon	Adenocarcinoma	2	IIIB	T4N1M0	Malignant
F	31	Colon	Adenocarcinoma	2	I	T2N0M0	Malignant
M	41	Colon	Adenocarcinoma	2	IIB	T4N0M0	Malignant
F	40	Colon	Adenocarcinoma	2	IIA	T3N0M0	Malignant
F	49	Colon	Adenocarcinoma	2	IIA	T3N0M0	Malignant
M	43	Colon	Adenocarcinoma	2	IIIB	T3N1M0	Malignant
M	61	Colon	Adenocarcinoma	2	IIIB	T3N1M0	Malignant
F	72	Colon	Adenocarcinoma	2	IIIB	T3N1M0	Malignant
F	69	Colon	Adenocarcinoma	2	IIA	T3N0M0	Malignant
M	73	Colon	Adenocarcinoma	3	IIA	T3N0M0	Malignant
M	55	Colon	Adenocarcinoma	2	I	T2N0M0	Malignant
F	62	Colon	Adenocarcinoma	2	IIB	T4N0M0	Malignant
F	60	Colon	Adenocarcinoma	2	IIIB	T3N1M0	Malignant
M	64	Colon	Adenocarcinoma	2	IIB	T4N0M0	Malignant
F	53	Colon	Adenocarcinoma	2	IIA	T3N0M0	Malignant
M	74	Colon	Adenocarcinoma	2	IIB	T4N0M0	Malignant
F	62	Colon	Adenocarcinoma	2	IIB	T4N0M0	Malignant
M	49	Colon	Adenocarcinoma	2	IIIB	T3N1M0	Malignant
F	62	Colon	Adenocarcinoma	2	IIB	T3N1M0	Malignant
F	55	Colon	Adenocarcinoma	2	IIB	T4N0M0	Malignant
M	82	Colon	Adenocarcinoma	2	IIA	T3N0M0	Malignant
F	60	Colon	Adenocarcinoma	2	IIA	T2N1M0	Malignant
F	42	Colon	Adenocarcinoma	2	IIA	T3N0M0	Malignant
F	49	Colon	Adenocarcinoma (sparse)	2	IIIB	T3N1M0	Malignant
M	47	Colon	Mucinous adenocarcinoma	3	IIA	T3N0M0	Malignant
F	54	Colon	Adenocarcinoma	2	IIIB	T4N1M0	Malignant
F	64	Colon	Adenocarcinoma	2–3	IIIC	T4N2M0	Malignant
F	55	Colon	Adenocarcinoma	2	IIA	T3N0M0	Malignant
M	51	Colon	Adenocarcinoma	3	IIA	T3N0M0	Malignant
F	56	Colon	Mucinous adenocarcinoma	2	IIIB	T3N1M0	Malignant
F	68	Colon	Mucinous adenocarcinoma	3	IIIB	T3N1M0	Malignant
M	78	Colon	Adenocarcinoma	3	IIA	T3N0M0	Malignant
M	48	Colon	Adenocarcinoma	3	IIIC	T4N2M0	Malignant

Supplementary Figure 1. Supplement to Figure 1. Detailed information of tissue microarray samples used for the EndoA3 expression analysis in Figure 1. **(A)** A representative image of isotype control (anti Rabbit IgG) for immunohistochemistry (IHC) staining on human tissue samples. **(B)** Human tumor samples for the IHC analysis (Figure 1) were obtained from US

Biomax (BC05118C). Grade 1 (well-differentiated) - cells appear normal and are not growing rapidly. Grade 2 (moderately-differentiated) - cells appear slightly different than normal. Grade 3 (poorly differentiated) - cells appear abnormal and tend to grow and spread more aggressively. Information regarding TNM grading is provided on the website at US Biomax.

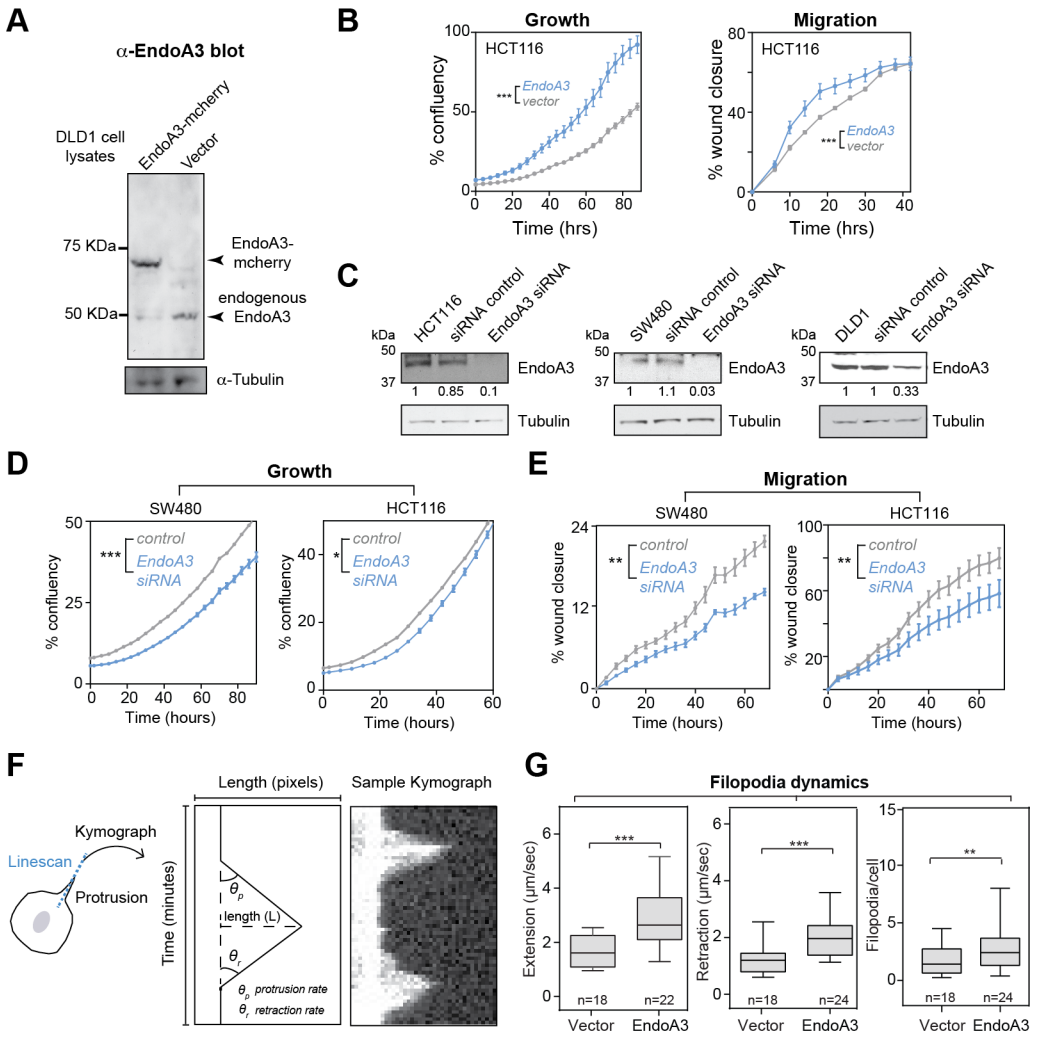

Supplementary Figure 2. Supplement to Figure 2 and Figure 3. **(A)** EndoA3-mCherry was expressed about 3 fold higher than endogenous EndoA3 in DLD1 cells. EndoA3 and EndoA3-mCherry were detected by an anti-EndoA3 antibody (Abcam) and were visualized using enhanced chemiluminescence (ECL). Tubulin signals were used as loading controls. **(B)** Adenocarcinoma HCT116 cells stably expressing EndoA3-mCherry grew (*left*) and migrate (*right*) faster than HCT116 cells carrying empty vectors. Data from 3 independent experiments were analyzed and plotted. Error bars indicate SEM. Two-way ANOVA was used for statistical analysis. *** *p<0.001*. **(C)** EndoA3 knockdown by siRNA in HCT116 (*left*), SW480 (*middle*), and DLD1 (*right)* colon adenocarcinoma cells was evaluated using western blots and ECL. Expression levels of EndoA3 (ratios between EndoA3 and tubulin signals) in siRNA treated cells were normalized to the EndoA3 level in untreated cells. Cell proliferation **(D)** and migration **(E)**

were decreased in the EndoA3 knockdown cells (blue), compared to cells expressing control siRNAs with scrambled sequence (gray). Data were collected from three independent biological repeats. Two-way ANOVA was used for statistical analysis. * *p<0.05; ** p<0.01; *** p<0.001*. **(F)** Quantification of protrusion dynamics using a kymograph analysis. A schematic diagram illustrates the kymograph analysis (Burdisso et al., 2013; Doyle et al., 2012; Sidani et al., 2007) in the *left* panel. Slope of the protrusion event (θ_p) indicates the protrusion rate, and slope of retraction event (θ_r) indicates retraction rate. Length of protrusion was calculated by measuring the distance from the edge of the cell boundary to tip of the protrusion (L) (*middle*). Representative kymograph of Lifeact-eGFP in EndoA3 DLD1 cells was obtained using Image J (*right*). **(G)** Quantification of protrusion extension rates (*left*), retraction rates (*middle*), and the number of *de novo* protrusions (*right*). Unpaired Student's t-tests were used for statistical analysis (** *p<0.01*, and *** *p<0.001*). '*n*' = number of cells analyzed. Data from three independent collections were used for these analyses.

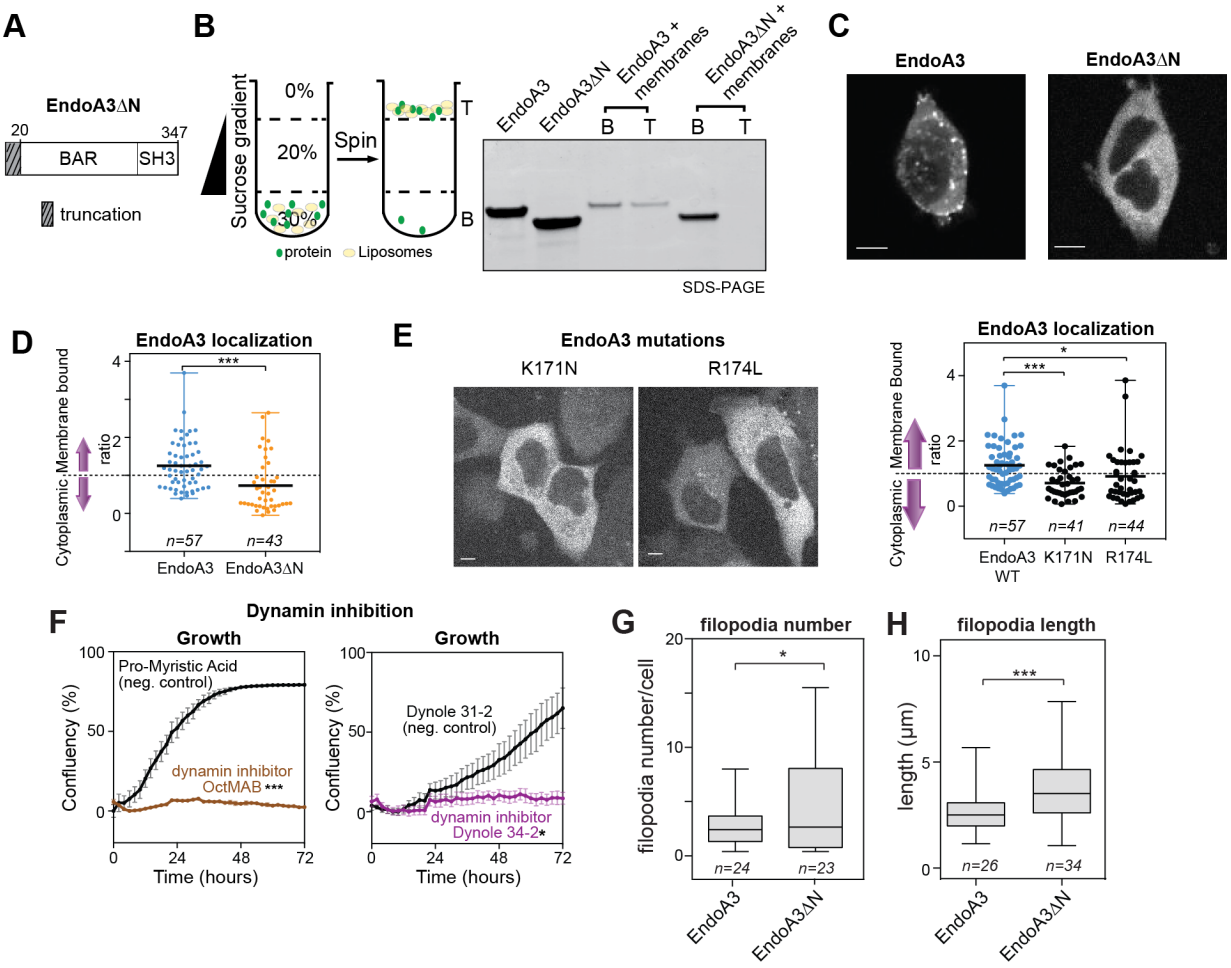

Supplementary Figure 3. Supplement to Figure 4**. (A)** EndoA3ΔN is a truncated version of EndoA3 that lacks the N-terminal 20 amino acid residues. **(B)** Sucrose gradient flotation assay (*left*) was used to examine EndoA3-membrane interactions (*right*). Liposome flotation assay was carried out as previously described (Poudel et al., 2016). EndoA3 (2 μM), TIAM1 (5 μM), and liposomes (2 mM total lipids, 1%PIP2, 25%PS, 5%NBD-PE, and 69%PC) were incubated at room temperature for 5 min. Samples were loaded to the bottom of a sucrose gradient, were centrifuged in SW 55-Ti rotor (Beckman) at 55,0000 rpm for 2 hrs, and were analyzed using SDS-PAGE. The left two lanes indicate total EndoA3WT and EndoA3ΔN used in the assay. The middle two lanes indicate bottom (B) and top (T) fractions of EndoA3 WT samples. The right two lanes indicate bottom and top fractions of EndoA3ΔN samples. **(C)** Representative images of

EndoA3-mCherry (*left*), EndoA3ΔN-mCherry (*middle*) are shown. Scale bars are 5μm. **(D)** The ratio between cytoplasmic and membrane-bound EndoA3 fractions are quantified and plotted. "n" = number of cells analyzed using fluorescence microscopy, *** $p<0.001$, unpaired Student's t-test. **(E)** Representative images and localization quantification of two mutant versions (K171N and R174L) of EndoA3 in DLD1 cells. Scale bars are 5μm. "n" = number of cells analyzed, *** $p<0.001$, and * $p<0.05$, unpaired Student's t-test. **(F)** Inhibition of endocytosis blocked the proliferation of EndoA3-DLD1 cells. Dynamin inhibitors OctMAB (a PH domain targeting inhibitor; 7μM, *left*) and Dynole 34-2 *(a* GTPase allosteric inhibitor; 5μM, *right*) were added to EndoA3 DLD1 cells. Cell growth was measured using the automated assay described in Figure 2. Error bars indicate SEM. Dynamin inhibitors and their negative controls (pro-myristic acid and dynole 31-2) were obtained from Abcam. * *p<0.05;* *** *p<0.0001.* **(G-H)** Filopodia dynamics in EndoA3 and EndoA3ΔN DLD1 cells. Actin-rich filopodia were visualized using lifeact-EGFP. The number of *de novo* protrusions formed in 10 min per cell was shown in **(G)**. The protrusion length was quantified in **(H)**. Kymograph based analysis was performed as described in Supplementary Figure 2 and Materials and Methods. Unpaired Student's t-tests were used for statistical analysis (* $p<0.05$, ** $p<0.01$, and *** $p<0.001$), '*n.s.*' = not significant, and '*n*' = the number of cells analyzed.

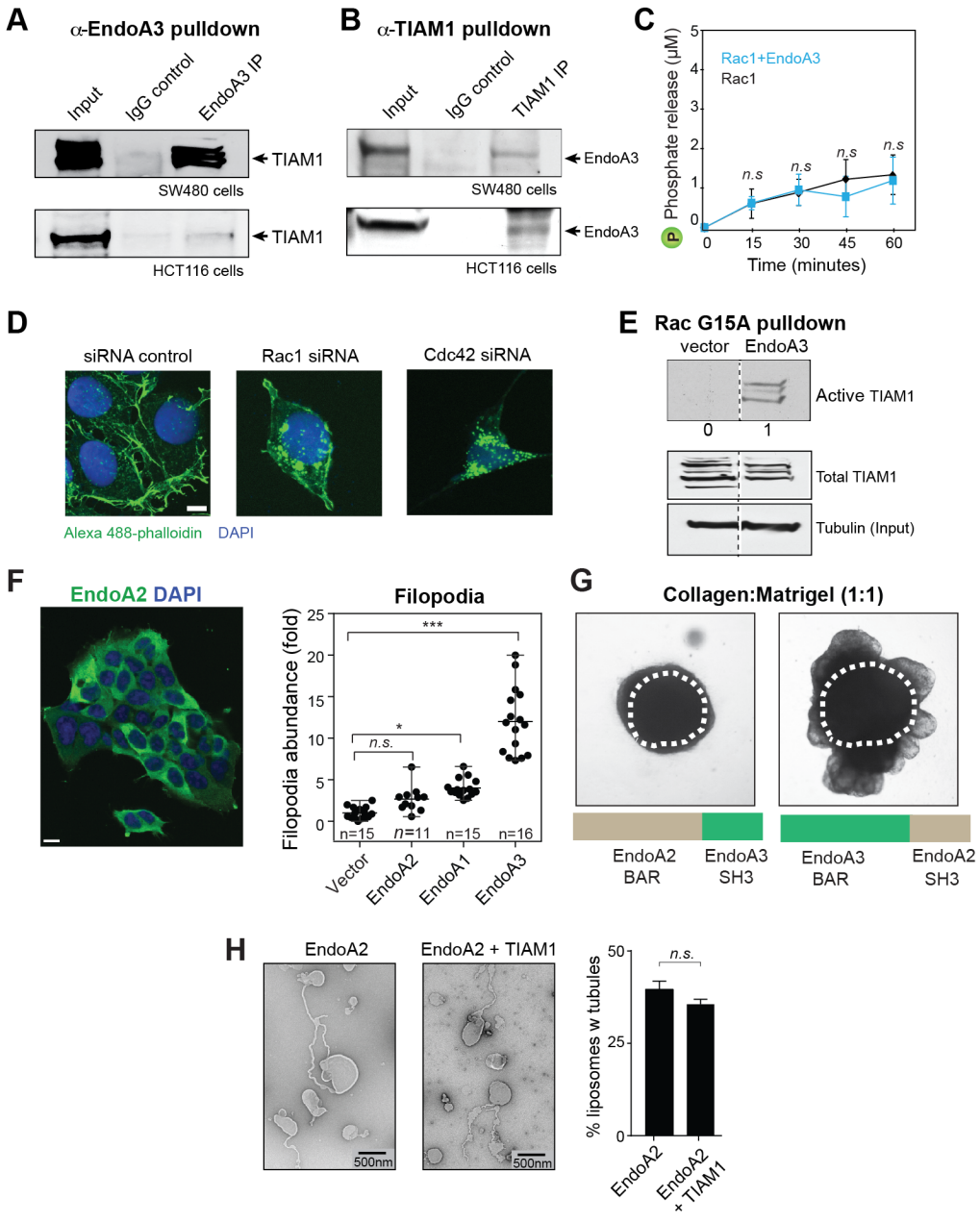

Supplementary Figure 4. Supplement to Figure 5. Endogenous EndoA3 and TIAM1 form complexes in SW480 **(A)** and HCT116 cells **(B)**. Lysates of SW480 and HCT116 cells were used for co-immunoprecipitation experiments. *Upper panels*: A mouse monoclonal antibody against EndoA3 (Santa Cruz Biotech.) was used to immunoprecipitate endogenous EndoA3, and TIAM1 was visualized using a rabbit polyclonal antibody against TIAM1 (Santa Cruz Biotech.) and enhanced chemiluminescence. *Lower panels*: A mouse monoclonal antibody against TIAM1 (Santa Cruz Biotech.) was used to immunoprecipitate endogenous TIAM1.

EndoA3 was visualized using a rabbit polyclonal antibody against EndoA3 (Abcam). Mouse IgG was used as controls for immunoprecipitation experiments. Co-immunoprecipitation signals for EndoA3 and TIAM1 from HCT116 cells were weak, likely due to low levels of endogenous EndoA3 in these cells (data not shown). **(C)** In the absence of TIAM1, the EndoA3 BAR domain failed to stimulate Rac1 GTPase activity. Malachite green assay was performed as described in Figure 5. **(D)** Knockdown either Rac1 or Cdc42 blocks filopodia formation in EndoA3-mCherry DLD1 cells; control (*left*), siRNA against Rac1 (*middle*), and siRNA against CDC42 (*right*). **(E)** Active TIAM1 levels were increased in EndoA3 DLD1 cells. GST-tagged Rac1 G15A mutant was used to pull-down active TIAM1 from lysates of EndoA3 DLD1 and control DLD1 cells. Samples were subjected to SDS-PAGE analysis. TIAM1 was visualized using a mouse monoclonal antibody against TIAM1 (Fred Hutchinson Share Resource) and ECL. **(F)** Endophilin isoforms exhibit specificity in promoting protrusions and migration. Retroviral transduction was used to express FLAG-tagged EndoA1, EndoA2, and EndoA3 in DLD1 cells. A representative image of EndoA2 DLD1 cells that were stained by DAPI (blue) and immunostained by a mouse monoclonal antibody against the FLAG-tag (green). Scale bar is 10 μm. The number of protrusions in EndoA1, EndoA2, and EndoA3 cells was quantified as described in Figure 3. Experiments were repeated 5 times. Error bars represent SEM and Student's t-tests were used for statistical significance analysis. '*n.s'* = not significant, *** $p<0.001$, ** $p<0.01$, and * $p<0.05$. **(G)** DLD1 cells that express chimeric proteins (EndoA2_BAR + EndoA3_SH3; *left*) and (EndoA3_BAR + EndoA2_SH3; *right*) were assayed for their 3-D motility. Representative images showing 3D spheroids at day 7, after being embedded into mixed Matrigel and collagen gels (1:1 volumetric ratio). Dotted circles indicate the initial size of the spheroid at day 1. **(H)** TIAM1 does not disrupt EndoA2-induced membrane tubulation. Membrane tubulation was visualized using transmission electron microscopy. EndoA2 (1 μM) was incubated with liposomes (0.5 mM total lipids; 74%PC, 25%PS, 1% PIP2) in the absence (*left*) and presence (*middle*) of 20 μM recombinant TIAM1 fragment. The percentage of

liposomes with membrane tubules was quantified (*right*). Student's t-test was used for statistical analysis. Three independent experiments were used for analysis.

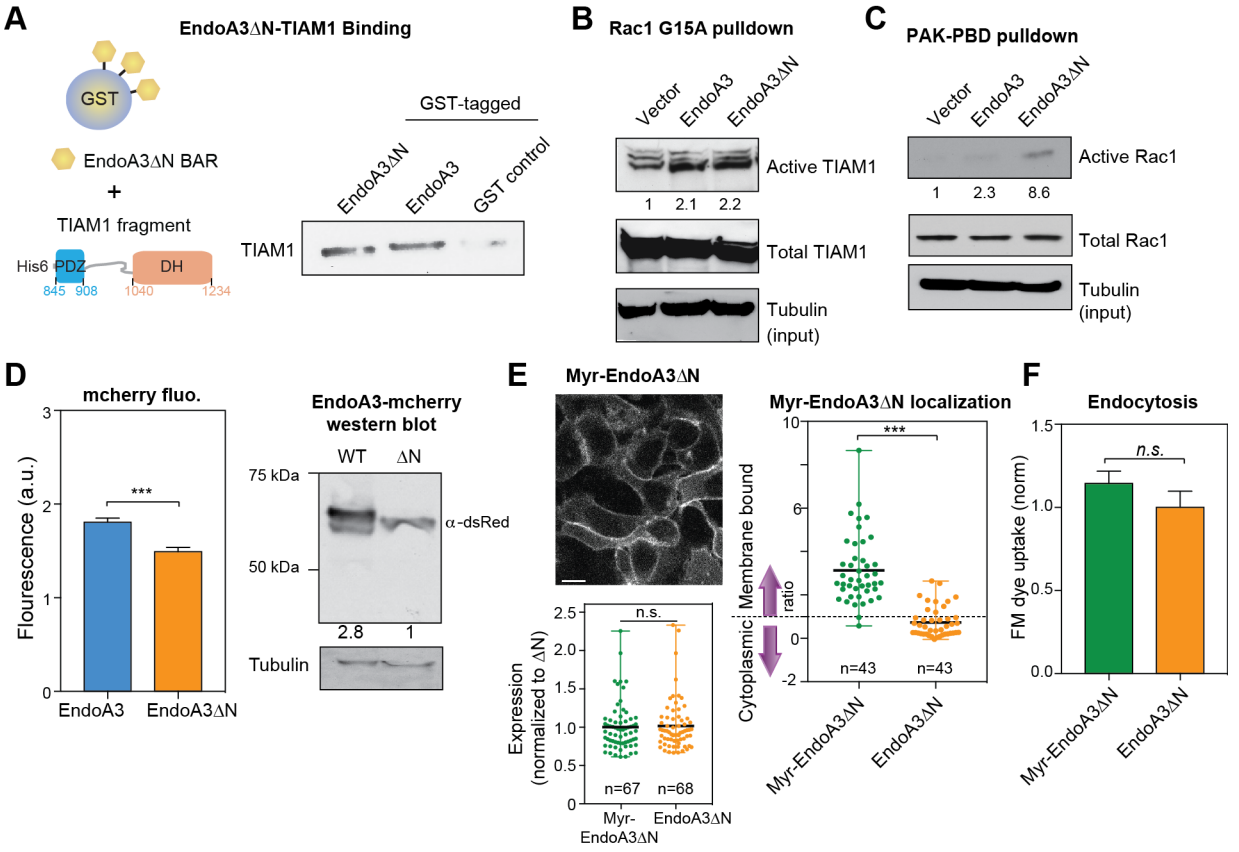

Supplementary Figure 5. Supplement to Figure 6. **(A)** Pull-down assays that show that GST-tagged EndoA3ΔN binds the recombinant his6-TIAM1 fragment. His6-TIAM1 was visualized using a monoclonal antibody against the his6-tag (Sigma-Aldrich) and ECL. GST pull-down assays were performed as described in Figure 5A. **(B)** Endogenous TIAM1 was activated upon EndoA3WT and EndoA3ΔN expression. Active TIAM1 was pulled down using a Rac1 G15A mutant from EndoA3WT and EndoA3ΔN cells, as described in Figure 6. **(C)** Rac1 activation was enhanced by EndoA3ΔN expression. Active Rac1 was pulled down using GST-tagged PAK PBD beads from EndoA3WT and EndoA3ΔN DLD1 cell lysates. Rac1 was detected using a mouse monoclonal antibody against Rac1 (Cytoskeleton Inc.) and enhanced chemiluminescence. Signals of Rac1 bands were normalized to tubulin. **(D)** Expression levels of EndoA3ΔN-mCherry and EndoA3-mCherry were quantified using mCherry fluorescence (*left*) and western blots against mCherry (anti-dsRed rabbit polyclonal) and ECL (*right*). **(E)** A representative image (*left upper*) and

quantified data (*right*) show that myr-EndoA3ΔN-GFP preferentially localizes to the plasma membrane. Expression levels of Myr-EndoA3ΔN-GFP and EndoA3ΔN-GFP were quantified using fluorescence signals (*left lower*). **(F)** FM4-64 dye uptake assay showed that EndoA3ΔN and myr-EndoA3ΔN cells exhibited similar levels of endocytosis.

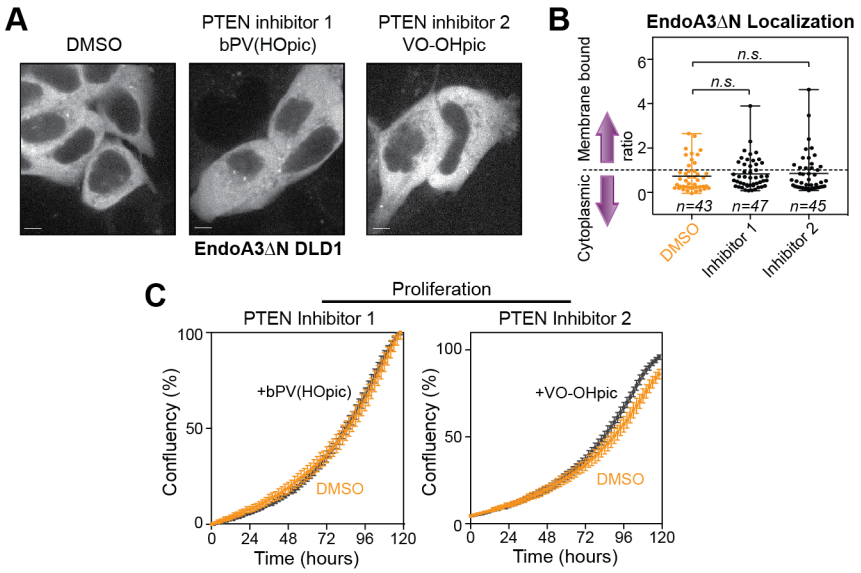

Supplementary Figure 6. Supplement to Figure 6. (A) PTEN inhibitors did not alter EndoA3ΔN localization. Representative images of EndoA3ΔN-GFP cells that were treated with DMSO (*left*), PTEN inhibitor 1 (bpV(HOpic), 200 nM; *middle*), or PTEN inhibitor 2 (VO-OHpic,200 nM; *right*) are shown in the panel A. **(B)** Ratios between membrane-bound and cytoplasmic EndoA3 were measured using ImageJ as described in Figure 6. "n" = the number of cells analyzed. ** $p<0.01$, one-way ANOVA. **(C)** Inhibition of PTEN did not affect the growth of EndoA3ΔN DLD1 cells (4 independent experiments, Two-way ANOVA, n.s.).

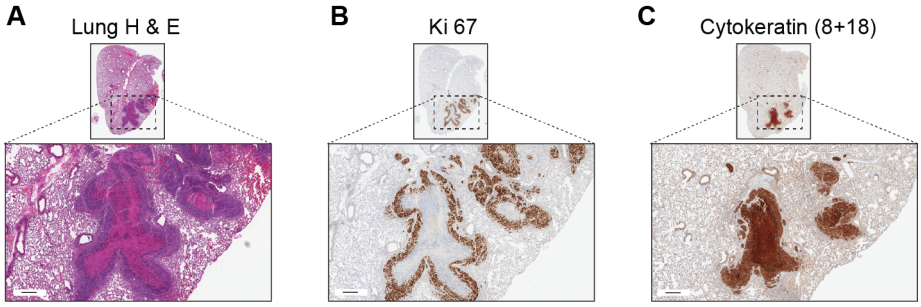

Supplementary Figure 7. Supplement to Figure 7. Representative IHC images of lung sections from mice carrying EndoA3WT DLD1 cells. **(A)** Metastatic nodules were visualized using H&E staining. **(B)** Proliferation at the site of metastatic nodules was observed using Ki-67 IHC. **(C)** Cytokeratin (CK8/18) IHC was used to confirm epithelial signature of the metastasized cells. Scale bars are 250 μm.

Supplementary Video 1. Supplement to Figure 4. **Dynamic distribution of EndoA3 between membrane and cytosol was disrupted by the amphipathic helix truncation.** Time-lapse videos of EndoA3-mcherry (*left*) and EndoA3DeltaN-mcherry (*right;* DeltaN = ∆N) DLD1 cells were recorded for 10 minutes (1 frame per 10 sec) and played at 10 frames per second.